Monthly Notices of the ROYAL ASTRONOMICAL SOCIETY

MNRAS **545,** 1–14 (2026) https://doi.org/10.1093/mnras/staf2057
Advance Access publication 2025 November 22

A search for transit-timing variations in the transiting hot-Jupiter systems HIP 65, NGTS-6, NGTS-10, and WASP-173

A. W. Griffiths [1★] J. Southworth [1★] L. Alegre [2,3] F. Amadio,[4] M. I. Andersen,[5] A. J. Barker [6] M. Basilicata,[7] M. Bonavita,[4] V. Bozza,[8,9] M. J. Burgdorf,[10] R. E. Cannon [2] G. Columba,[11] M. Dominik [12] A. Donaldson,[2] R. Figuera Jaimes,[12,13,14,15] T. C. Hinse [16] M. Hundertmark,[17] U. G. Jørgensen,[4] E. Khalouei,[18] P. Longa-Peña,[19] L. Mancini [7,20,21] F. Manni,[7] B. Murphy,[2] N. Peixinho,[22] M. Rabus [23] S. Rahvar [24] H. Rendell-Bhatti,[2] P. Rota,[8] A. Rożek,[2] S. Sajadian,[24] J. Skottfelt,[25] C. Snodgrass [2] and J. Tregloan-Reed[19]

Affiliations are listed at the end of the paper

Accepted 2025 November 16. Received 2025 November 14; in original form 2025 June 10

ABSTRACT

Hot Jupiters are Jupiter-mass planets with orbital periods of less than 10 d. Their short orbital separations make tidal dissipation within the stellar host especially efficient, potentially leading to a measurable evolution of the orbit. One possible manifestation of this is orbital decay, which presents itself observationally through variations in the orbital period and thus times of transit. Here, we select four promising exoplanetary systems for detecting this effect: HIP 65, NGTS-6, NGTS-10, and WASP-173. We present 33 new transit light curves taken with the 1.54 m Danish Telescope, and analyse these alongside photometric data from the *Transiting Exoplanet Survey Satellite* and transit-timing data from the literature. We construct two ephemeris models for each target: a linear ephemeris and a shrinking orbital period due to tidal decay. The linear ephemeris is preferred for three of the four models – the highest significance for the quadratic ephemeris is over 3σ for WASP-173. We compare these results to theoretical predictions for tidal dissipation of gravity waves in radiation zones, and find that wave breaking is predicted only in WASP-173, making rapid decay plausible in this system but unclear in the other three. The sensitivity of transit timings to orbital decay depends on the square of the time interval covered by available observations, so our results establish a useful baseline against which future measurements can be compared. NGTS-6 and NGTS-10 are important objects for future study as they are in the first field to be observed by the upcoming *PLATO* mission.

Key words: techniques: photometric.

1 INTRODUCTION

Hot Jupiters, classified based on their large masses and short orbital periods, are a relatively rare type of exoplanet within the underlying population (A. W. Howard et al. 2010, 2012; M. Mayor et al. 2011). Despite their scarcity, they make up a significant fraction of the known exoplanets (B. S. Gaudi et al. 2002; J. T. Wright et al. 2012). This is a consequence of their relatively large sizes and small semimajor axes making them the easiest transiting planets to detect. This proximity to the host star raises tides on both bodies, causing tidal bulges (C. D. Murray & S. F. Dermott 1999).

For a planet in an asynchronous orbit – one in which the planet's spin period is not equal to the orbital period – the motion of the tidal bulges is opposed by viscous friction. This dissipation of energy transfers angular momentum from the planetary orbit to the stellar spin. In the typical case for a hot Jupiter, where its orbital period is shorter than the host star's spin period, tidal effects spin-up the star and shrink the orbit (P. Hut 1980, 1981). The eventual outcome of sustained orbital shrinkage is the planet slowly spiralling into the star in a process called tidal decay (C. C. Counselman 1973). It is worth noting that there are various contributions to tidal dissipation (F. A. Rasio et al. 1996), but arguably the largest is that of the wave-like dynamical tide (A. J. Barker 2020).

Tidal decay in exoplanets is not easily detectable. There is currently no confirmed way to measure the spin or internal density distribution of exoplanets, which would otherwise give information on the tidal mechanisms and angular momentum transfer within the system. However, some claims have been made for the observation of oblateness brought on by tides (e.g. Q. Liu et al. 2024; E. M. Price et al. 2025; J. J. Zanazzi & E. Chiang 2025). The time-scales on which tides act are also unknown and it has been argued that the circularization of transiting exoplanets may not be entirely due to tides (B. Levrard, C. Winisdoerffer & G. Chabrier 2009).

Presently, signs of tidal decay have only been detected through transit-timing variations (TTVs; E. Agol & D. C. Fabrycky 2018), which show variations in the times of mid-transit and a decrease

★ E-mail: a.w.griffiths@keele.ac.uk (AWG); taylorsouthworth@gmail.com (JS)

in the orbital period of the planet over time. The associated change in period is measurable from transit light curves and allows for the determination of the modified tidal quality factor, $Q'_\star$, providing an insight into the rate of energy dissipation within the star due to tides. $Q'_\star$ is defined as follows:

$$Q'_\star = \frac{3Q_\star}{2k_2} \tag{1}$$

where k_2 is the Love number (A. E. H. Love 1911) and $Q_\star$ is the tidal quality factor – linked to the dissipation of tidal energy through the equation (P. Goldreich & S. Soter 1966):

$$Q_\star = \frac{1}{2\pi E_0} \oint \left(-\frac{\mathrm{d}E}{\mathrm{d}t} \right) \mathrm{d}t \tag{2}$$

where E_0 is the maximum energy stored in a tide, $-\mathrm{d}E/\mathrm{d}t$ is the dissipation rate, and the integral is over one tidal cycle. While a negative period derivative can be a response to the tidal evolution of the system, this effect can be caused by other phenomena such as the light-time effect, in which a wide-orbiting third body causes the star–planet pair to orbit the system's barycentre (J. B. Irwin 1952), and apsidal motion, arising only in orbits with non-zero eccentricity. Both phenomena are periodic so can be distinguished from tidal decay over a large enough time-scale.

WASP-12 b, a 1.5 $M_{\rm Jup}$ hot Jupiter orbiting an F-type main-sequence star (L. Hebb et al. 2009), was until recently the sole confirmed case of tidal decay in exoplanets (G. Maciejewski et al. 2016; S. W. Yee et al. 2020; J. D. Turner, A. Ridden-Harper & R. Jayawardhana 2021). Since the confirmation of the system's shrinking orbital period, the decay rate has been refined multiple times (L. Bai et al. 2022; J. D. Turner et al. 2022; I. Wong et al. 2022; A. C. Kutluay et al. 2023; A. S. Nediyedath et al. 2023; B. Akinsanmi et al. 2024; P. Leonardi et al. 2024; W. Wang et al. 2024). A recent study by L. M. Bernabò et al. (2025) has detected orbital decay within WASP-43, making it the second confirmed hot-Jupiter system. Despite the contemporary exclusivity of these systems, there are many candidates for tidal decay, with few having established TTVs.

One such candidate is WASP-4 b (D. M. Wilson et al. 2008), for which TTVs were first detected by L. G. Bouma et al. (2019). These authors suggested the apparent period change could be caused by tidal decay, apsidal precession, or gravitational perturbation from another body. J. Southworth et al. (2019) refined the rate of period shrinkage and ruled out stellar activity and the Applegate mechanism (J. H. Applegate 1992). L. G. Bouma et al. (2020) and J.-V. Harre & A. M. S. Smith (2023) investigated the possibility of a line-of-sight acceleration, attributed to a distant perturbing body. With their new transit-timing data, Ö. Baştürk et al. (2025) established that the discrepancies would be best explained by tidal orbital decay. However, the TTVs of the WASP-4 system are now believed to be associated with the light-time effect (J. N. Winn & G. Stefánsson 2025).

1.1 Target selection

The magnitude of detectable orbital decay within hot-Jupiter planetary systems can be quantified using the transit time-shift equations presented by J. L. Birkby et al. (2014) and G. Maciejewski et al. (2018):

$$T_{\rm shift} = -\frac{27}{4}\frac{\pi}{Q'_\star}\left(\frac{M_{\rm p}}{M_\star}\right)\left(\frac{R_\star}{a}\right)^5\left(\frac{1}{P}\right)(10\mathrm{yr})^2 \tag{3}$$

where $T_{\rm shift}$ is the shift in transit mid-points over 10 yr, $M_\star$ and $M_{\rm p}$ are the respective stellar and planetary masses, $R_\star$ is the stellar radius, a is the orbital semimajor axis, and P is the orbital period. Here, $Q'_\star$ is set to a canonical value of 10^6 (G. I. Ogilvie 2014). Whilst requiring some preliminary spectroscopic parameters, this equation allows systems with the most favourable predicted time-shifts to be selected for analysis.

We used this equation to select targets with the largest $T_{\rm shift}$. We then restricted the sample based on sky position to include only those objects with good observability for the available telescope time. A nominal lower limit of 10 s was specified for $T_{\rm shift}$, but objects close to this limit were ultimately not observed due to the limited availability of telescope time. The first result of this project was an analysis of HATS-18 (J. Southworth et al. 2022); see also a study of KELT-16 by L. Mancini et al. (2022).

1.1.1 HIP 65 Ab

Our first target is HIP 65, a wide binary star system hosting a K-dwarf (HIP 65 A) and an M-dwarf (HIP 65 B). The hot-Jupiter planet HIP 65 Ab orbits the K-dwarf with an ultrashort period of 0.981 d (L. D. Nielsen et al. 2020; L. A. Paredes et al. 2021). HIP 65 A and HIP 65 B are separated by 3.95 arcsec on the sky (L. D. Nielsen et al. 2020), corresponding to a projected separation of 269 au. These authors highlighted the planet's large impact parameter and grazing eclipse, making radius estimations unreliable. They stated also that HIP 65 Ab is one of very few massive planets that reside within twice their Roche limit, lying on the border of the Neptune desert (G. M. Szabó & L. L. Kiss 2011). However, its exact relation to the Roche limit is uncertain due to the grazing eclipses. L. D. Nielsen et al. (2020) also report HIP 65 A's rotation period as $13.2^{+1.9}_{-1.4}$ d from rotational modulation in light curves, and suggest tidal spin-up due to the discrepancy between the gyrochronological ($0.32^{+0.10}_{-0.06}$ Gyr) and isochronal ($4.1^{+4.3}_{-2.8}$ Gyr) ages of the star. However, the isochronal ages of K-dwarfs are unreliable so this is not in itself evidence of tidal evolution (P. F. L. Maxted, A. M. Serenelli & J. Southworth 2015; but see also R. A. Tejada Arevalo, J. N. Winn & K. R. Anderson 2021).

Photometric data on HIP 65 Ab from the *Transiting Exoplanet Survey Satellite* (*TESS*; G. R. Ricker et al. 2015) have previously been examined for eclipse depth variations (E. Gal-on et al. 2022; G. Wang & N. Espinoza 2024), with the purpose of tracking its atmospheric activity. No eclipse depth variations were found after fixing the impact parameter; as such, the grazing eclipse was likely responsible for the initial variations.

Using equation (3), we find HIP 65 Ab to be a promising candidate for detecting tidal decay, having an estimated $T_{\rm shift}$ of -23.7 ± 2.2 s in 10 yr (s in 10 yr). In spite of the promise of this system, there have been two previous orbital decay searches of HIP 65 Ab with limited success. E. R. Adams et al. (2024) found a period increase of 22.3 ± 9.6 ms yr^{-1} using 106 transit times spanning five years. G. Maciejewski et al. (2024) found the decay rate to be $(-0.1 \pm 3.1) \times 10^{-10}$ d per orbital cycle. Both studies were limited by the data available at the time, with the majority of their transit mid-points originating from *TESS*. Here, we use new precise transit photometry alongside *TESS* to search for variations in transit timing.

1.1.2 NGTS-6 b

Our second target is an ultrashort-period hot Jupiter orbiting an old K-dwarf. NGTS-6 b (J. I. Vines et al. 2019) is the least

massive planet in our sample, 1.3 M_{Jup}, and has an orbital period of 0.882 d. The estimated orbital decay associated with this planet is $T_{shift} = -19.1 \pm 13.7$ s in 10 yr. A. J. Barker (2020) suggested that the stellar host likely experiences no wave breaking, so rapid decay is not expected. However, photometric observations may provide signs of tidal decay in the event that its internal gravity waves are fully damped. This exoplanet also orbits near Roche contact (V. Antonetti & J. Goodman 2022) similar to the case of HIP 65 Ab.

1.1.3 NGTS-10 b

NGTS-10 b is a 2.16 M_{Jup} planet with an ultrashort period of 0.767 d and had the shortest known period of any hot Jupiter at the time of discovery (J. McCormac et al. 2020). Its stellar host is an old K-type star of mass 0.70 $M_{\odot}$, which has a rotation period of 17.3 d. There have been various theoretical studies of the system, some investigating its atmosphere and climate (e.g. C. Helling et al. 2023; J. A. Kappelmeier, R. J. MacDonald & N. K. Lewis 2024), and some investigating the effects of tides (e.g. A. J. Barker 2020; J. A. Alvarado-Montes et al. 2021; T. Tokuno, A. Fukui & T. K. Suzuki 2024). NGTS-10 b is an interesting object for several research areas, particularly orbital decay. We estimate a large T_{shift} of -62.8 ± 29.9 s in 10 yr, but as with NGTS-6, no wave breaking or rapid decay is projected (A. J. Barker 2020).

1.1.4 WASP-173 Ab

WASP-173 Ab (KELT-22 A) is a hot Jupiter orbiting a solar-type star, and is notable for being discovered by two independent consortia simultaneously (C. Hellier et al. 2019; J. Labadie-Bartz et al. 2019). Similarly to the HIP 65 system, its host star has a distant binary companion, this time at 1400 au. WASP-173 Ab is an inflated planet, with a mass of 3.7 M_{Jup}, a radius of 1.2 R_{Jup}, a period of 1.39 d, and an irradiation level significantly more than the threshold for inflation (B.-O. Demory & S. Seager 2011; J. Labadie-Bartz et al. 2019). Its stellar host is a G-type star with a rotation period of around 8.4 d (E. Knudstrup et al. 2024).

This planet has seen little individual attention since its discovery, mostly being included in tide-related projects with substantial sample sizes (e.g. R. A. Tejada Arevalo et al. 2021). The linear ephemeris has been refined numerous times in previous large-scale studies (e.g. E. S. Ivshina & J. N. Winn 2022; A. Kokori et al. 2023; S.-S. Shan et al. 2023) and analysed for timing variations (E. R. Adams et al. 2024; G. Maciejewski et al. 2024), with many suggesting it is a good candidate for tidal decay (e.g. K. C. Patra et al. 2020; N. N. Weinberg et al. 2024). With the time-shift equation, we estimate a period decay of -23.9 ± 6.6 ms over the next 10 yr and contrast it with the increase in orbital period found by E. R. Adams et al. (2024) of 19.3 ± 11.0 ms yr^{-1}, and that of $(1.1 \pm 5.2) \times 10^{-10}$ d per cycle by G. Maciejewski et al. (2024). We aim to refine these prior studies with the addition of our new transit light curves, whilst also providing data for future work in this area.

2 OBSERVATIONS

2.1 Danish 1.54-m Telescope

All new ground-based observations in this work were obtained using the 1.54 m Danish Telescope at ESO La Silla, Chile, as a side-project of the MiNDSTEp microlensing observations (M. Dominik et al. 2010). The Danish Faint Object Spectrograph and Camera was used in imaging mode, in which form it is equipped with a 2048×2048 pixel CCD camera with a 13.7′ field of view sampled at 0.39 arcsec $pixel^{-1}$. The CCD was windowed to decrease the readout time in all cases. The filters used were Johnson V, Bessell R, and Bessell I. Some of the observations were obtained with the telescope moderately defocused to improve the precision of the observations, following the method set out by J. Southworth et al. (2009a). An observing log is given in Table 1. All observations in the log were included in the timing analysis.

HIP 65 is a bright star ($V = 11.1$) and the planet produces a short (47 min) and shallow (0.6 per cent) eclipse. We experimented with using different filters and focus levels, in some cases pre-planned and in others as a response to the sky conditions during an observing sequence. The majority of our observations were, in the end, obtained through the I filter and with moderate defocus, and achieved a photometric precision in the region of 1 mmag per point.

NGTS-6 is rather fainter ($V = 14.1$) and has a companion at an angular distance of 5.4 arcsec. The majority of our observations were taken with no or small defocus, and through the I filter to lower the count rate. When the seeing was good we were able to extract light curves of NGTS-6 without contamination by the fainter nearby star.

NGTS-10 is another relatively faint star ($V = 14.3$), but without a nearby companion. In all our observing sequences, we used an R filter to maximize throughput, and moderate defocusing with exposure times of 60–100 s. The photometric precisions obtained are in the region of 1.5 mmag per point.

WASP-173 is a bright star ($V = 11.2$) with a fainter companion at 6.0 arcsec. When the observing conditions were good we used short exposure times and operated the telescope in focus to extract light curves of WASP-173 without contamination. In times of poorer seeing we defocused the telescope and increased the exposure time, with the intention of recording light curves of the combined light of WASP-173 and its companion. This means some of our light curves accurately reflect the properties of WASP-173 itself, whereas some suffer from third light which causes a smaller transit depth.

The data were reduced using the DEFOT pipeline (J. Southworth et al. 2009b, 2014), which in turn uses the IDL[1] implementation of the APER routine from DAOPHOT (P. B. Stetson 1987) contained in the NASA ASTROLIB library[2] to perform aperture photometry. We constructed master bias and flat-field images but did not apply them to the data because their main effect was to add to the scatter in the light curves without modifying the shape of the transit. A differential-magnitude light curve was generated for each transit observation by constructing an optimal composite comparison star to calculate differential magnitudes against. The composite comparison star was made by iteratively adjusting the weights of individual stars and the coefficients of a low-order polynomial to minimize the scatter in the data outside transit.

The timestamps for the mid-point of each image were taken from the headers of the FITS files and converted to the BJD_{TDB} time-scale using routines from J. Eastman, R. Siverd & B. S. Gaudi (2010). Manual time checks were performed for many transits, in all cases confirming the reliability of the timestamps in the FITS headers.

[1] https://www.ittvis.com/idl/
[2] http://idlastro.gsfc.nasa.gov/

Table 1. Log of the transit observations obtained for this work. N_{obs} is the number of observations, T_{exp} is the exposure time, T_{dead} is the mean time between the end of one exposure and the start of the next, and 'Moon illum.' is the fractional illumination of the Moon at the mid-point of the transit. The aperture radii are target aperture, inner sky, and outer sky, respectively.

Target	Date of first observation	Start time (UT)	End time (UT)	N_{obs}	T_{exp} (s)	T_{dead} (s)	Filter	Airmass	Moon illumination	Aperture (pixels)
HIP 65	2021/09/20	04:32	07:17	230	30	11	*I*	1.11 → 1.26	0.992	11 20 40
HIP 65	2021/09/22	04:06	06:31	210	30	11	*I*	1.11 → 1.19	0.983	25 35 70
HIP 65	2022/09/15	05:17	06:46	75	60	12	*R*	1.11 → 1.17	0.747	20 32 70
HIP 65	2022/09/16	04:58	07:24	114	60	12	*V*	1.11 → 1.25	0.658	17 25 45
HIP 65	2022/09/21	02:51	05:14	165	40	12	*R*	1.19 → 1.11	0.212	22 32 70
HIP 65	2023/07/15	08:26	10:28	101	60	13	*I*	1.12 → 1.11 → 1.14	0.054	25 40 80
HIP 65	2023/07/17	07:21	09:48	122	60	13	*I*	1.17 → 1.11 → 1.12	0.003	25 35 80
HIP 65	2023/09/13	04:32	06:55	196	30	10	*I*	1.12 → 1.11 → 1.17	0.032	20 30 60
HIP 65	2024/07/18	04:31	06:50	261	20	9	*I*	1.67 → 1.21	0.878	20 30 60
HIP 65	2024/07/19	04:08	06:09	229	20	11	*I*	1.78 → 1.28	0.938	20 30 60
HIP 65	2024/09/04	06:21	08:15	420	5	10	*I*	1.11 → 1.25	0.014	12 24 40
NGTS-6	2019/08/23	07:11	10:26	235	40	10	*R*	1.90 → 1.04	0.524	8 18 35
NGTS-6	2019/09/07	07:53	10:01	80	80	11	*R*	1.24 → 1.03	0.630	19 28 50
NGTS-6	2019/09/15	07:24	09:58	125	60	14	*R*	1.23 → 1.00 → 1.24	0.986	8 20 50
NGTS-6	2021/09/25	05:11	07:15	156	30	15	*I*	1.65 → 1.14	0.832	7 20 40
NGTS-6	2021/10/02	06:12	08:29	187	30	13	*I*	1.24 → 1.01	0.202	8 19 40
NGTS-6	2022/10/11	06:05	08:00	97	35–60	14	*I*	1.16 → 1.01	0.977	7 18 35
NGTS-6	2023/10/05	05:54	07:53	148	30	14	*I*	1.26 → 1.02	0.667	13 22 50
NGTS-6	2024/09/05	07:48	09:59	175	30	13	*I*	1.27 → 1.02	0.047	9 19 40
NGTS-6	2024/09/13	06:27	08:20	178	30–20	13	*I*	1.51 → 1.10	0.711	8 20 40
NGTS-10	2022/09/12	07:17	09:52	103	100–55	12	*R*	1.71 → 1.07	0.951	8 12 50
NGTS-10	2022/09/22	06:39	09:08	79	100	14	*R*	1.70 → 1.08	0.128	9 25 40
NGTS-10	2023/10/09	04:36	08:27	125	100	13	*R*	2.46 → 1.05	0.256	15 22 40
NGTS-10	2023/10/12	06:32	08:28	63	100	11	*R*	1.28 → 1.03	0.056	9 12 17
NGTS-10	2024/09/18	07:10	09:32	85	60	13	*R*	1.57 → 1.06	0.999	6 12 50
NGTS-10	2024/09/28	06:21	09:38	13	60	13	*R*	1.64 → 1.01	0.172	8 25 40
WASP-173	2021/09/29	03:03	07:24	390	20	14	*R*	1.03 → 1.00 → 1.44	0.490	21 32 70
WASP-173	2022/07/06	05:19	08:42	244	30	17	*I*	1.59 → 1.01	0.419	7 38 52
WASP-173	2022/09/05	05:14	09:12	543	10–20	13	*I*	1.00 → 1.51	0.676	8 30 50
WASP-173	2023/08/01	06:02	10:16	835	5–4	13	*I*	1.08 → 1.00 → 1.20	0.995	8 25 50
WASP-173	2023/08/26	04:49	09:15	522	10	17	*I*	1.05 → 1.00 → 1.32	0.701	8 35 50
WASP-173	2024/07/03	04:52	09:22	317	30	13	*I*	1.91 → 1.00	0.083	8 30 50
WASP-173	2024/08/22	02:52	07:05	732	10–5	13	*I*	1.37 → 1.00 → 1.02	0.486	9 30 50

2.2 *Transiting Exoplanet Survey Satellite*

TESS data were extracted from the Mikulski Archive for Space Telescopes (MAST) archive[3] via the LIGHTKURVE package (Lightkurve Collaboration 2018). We exclusively used 120 s cadence observations from the Science Processing Operations Center (SPOC), with a standard bitmask. Pre-search Data Conditioning Simple Aperture Photometry fluxes were used where possible. The first and final 1 per cent of times in each light curve were discarded to remove any artefacts. We applied the Savitzky–Golay filter (A. Savitzky & M. J. E. Golay 1964) to remove low-frequency trends before the light curves were normalized. Fluxes were then converted to magnitude units. Each *TESS* sector was split into two, where the most central transit mid-point was taken from each half-*TESS* sector for the light curve and timing analyses.

HIP 65 A has been observed in six *TESS* sectors (1, 2, 28, 29, 68, and 69) spanning a five-year time interval, with our ground-based transit light curves adding an additional year. WASP-173 A has been observed in half as many sectors (2, 29, and 69), NGTS-6 was only observed in two sectors (5 and 32) and NGTS-10 has coverage from just one sector (87).

[3] https://mast.stsci.edu/portal/Mashup/Clients/Mast/Portal.html

3 ANALYSIS

3.1 Light-curve analysis

We used version 43 of the JKTEBOP code (J. Southworth 2013) to fit all light curves. Free parameters for our ground-based observations include the sum of fractional radii ($r_\star + r_p$, where $r_{\star,p} = \frac{R_{\star,p}}{a}$), ratio of the radii ($k = \frac{r_p}{r_\star}$), inclination ($i$), light scale factor, and time of mid-transit (T_{mid}). The orbital period (P) was also made a free parameter during light-curve fitting of *TESS* data. We applied the power-2 limb-darkening law (D. Hestroffer 1997), with coefficients interpolated from tabulations by A. Claret & J. Southworth (2022). These coefficients were kept fixed. We assume fixed circular orbits for all targets based on the adopted values established in all respective discovery papers, despite some small but non-zero eccentricity results from other sources (e.g. A. Kokori et al. 2023). All other initial and fixed transit parameters were

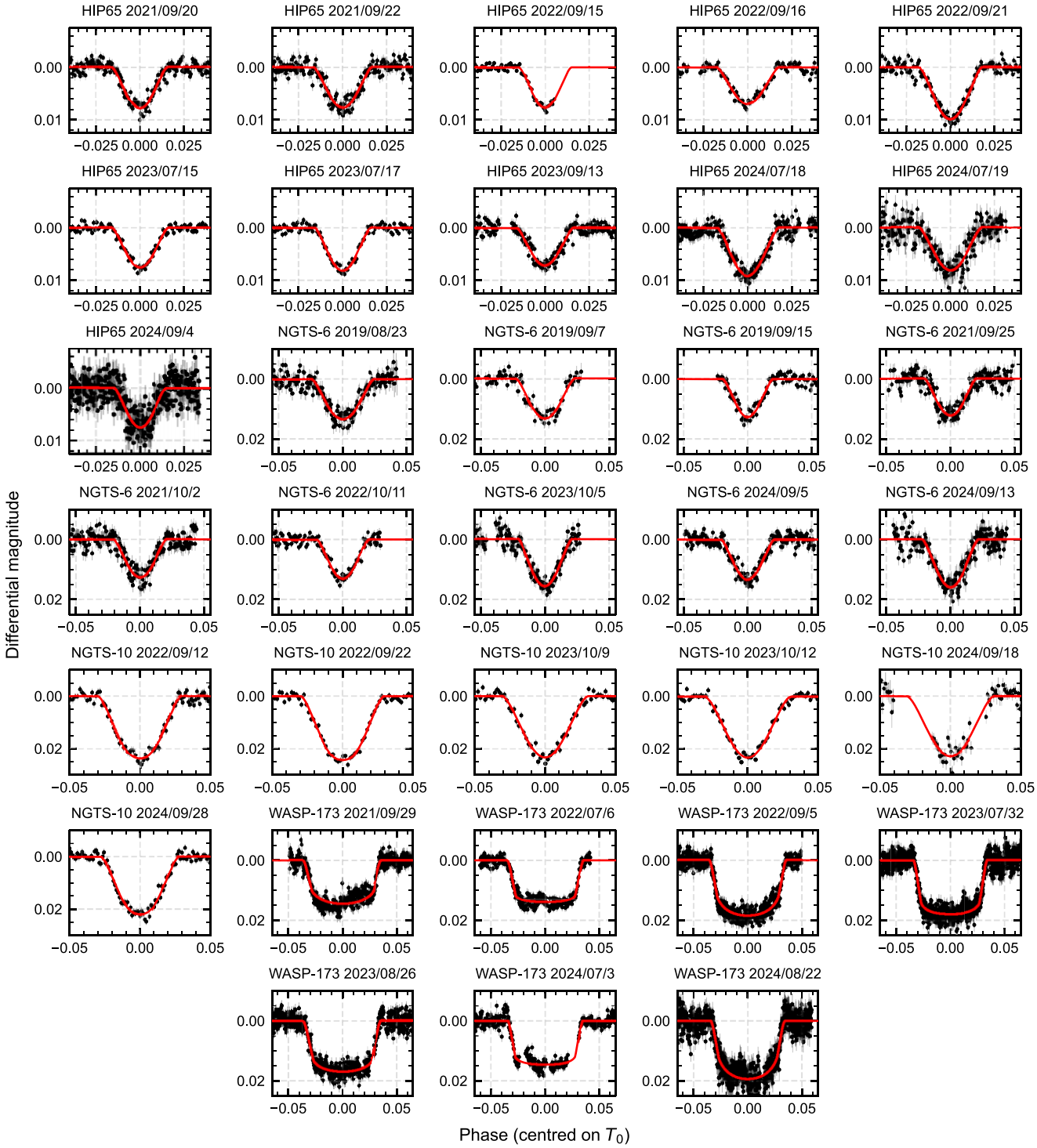

Figure 1. New transit light curves for HIP 65 A, NGTS-6, NGTS-10, and WASP-173 A taken with the Danish Telescope. Data points are displayed with their error bars. Fits are plotted in front of the data. The dates of observation are displayed above each plot.

taken from the respective discovery papers. Uncertainties on fitted parameters were calculated using both Monte Carlo and residual-shift methods in JKTEBOP (J. Southworth 2008). The residual-shift method assesses the importance of correlated noise, accounting for it in the error budget. The overall uncertainties on the mid-transit times were picked as the larger of the two multiplied by the corresponding reduced χ^2 value. Fig. 1 shows all new transit light curves from the Danish Telescope (those from TESS can be found in Appendix A).

3.2 Literature mid-times

We combined our transit times for HIP 65 Ab with an additional three from the literature. These come from the ExoClock Project

(A. Kokori et al. 2022a, b, 2023), an operation aiming to track the ephemerides of over 1000 transiting exoplanets. The three transit times were taken in succession with the Yves Jongen Telescope in Deep Sky Chile. Three transit times were also pulled from the Exoplanet Transit Database (ETD), a catalogue of transit light curves taken by amateur astronomers (S. Poddaný, L. Brát & O. Pejcha 2010).

Eight transit times of NGTS-6 b are available from the ExoClock Project: four from Yves Jongen at Deep Sky Chile, three from Jean–Pascal Vignes at Deep Sky Chile, and one from Anaël Wünsche at El Sauce Observatory. These times span the month of December in the year 2021. We refitted one light curve using data from the Next-Generation Transit Survey (NGTS) published in the planet's discovery paper (J. I. Vines et al. 2019) and three additional times were taken from the ETD. We note that six of the transit mid-points from ExoClock have an epoch in common with an ExoClock transit time. Since all common times are taken with different telescopes, we do not reject any of the data. The same applies to a transit time from the ETD which was obtained at the same epoch as one we observed with the Danish Telescope.

Available timing data for the NGTS-10 system is scarce. The only source in the literature is the discovery paper (J. McCormac et al. 2020), from which we obtain four transit mid-points by refitting the transit light curves. The resulting times were converted from $\mathrm{HJD_{UTC}}$ to $\mathrm{BJD_{TDB}}$ following the method described in Section 2.1. No data are currently available from ExoClock or the ETD.

In the case of WASP-173 Ab, one transit light curve was taken from the first discovery paper by C. Hellier et al. (2019) and refitted. Timing data were given in $\mathrm{HJD_{UTC}}$ and so were converted to $\mathrm{BJD_{TDB}}$. Three mid-transit times were presented in the second discovery paper (J. Labadie-Bartz et al. 2019). The ExoClock Project and ETD again both have timing data. We obtained one transit time from each.

3.3 Transit-timing analysis

We constructed linear and quadratic ephemerides to fit the timing data. The linear fit represents a constant-period orbit in a system with no orbital decay. It is described by

$$T_{\mathrm{mid}} = PE + T_0 \tag{4}$$

where P is the constant orbital period, E is the transit epoch, and T_0 is the value T_{mid} at $E = 0$. The quadratic fit represents an orbital decay model, but is also sensitive to the other aforementioned TTV mechanisms. This model is

$$T_{\mathrm{mid}} = pE^2 + PE + T_0 \tag{5}$$

and invokes a quadratic coefficient p, a quantity linked to the rate of period growth $\dot{P}$ by $p = \frac{1}{2}P\dot{P}$. A negative value of p indicates period shrinkage and possible tidal decay. Model parameters for both fits were estimated using a Markov Chain Monte Carlo (MCMC) method with the EMCEE package (D. Foreman-Mackey et al. 2013), where the quadratic coefficient p was allowed to be positive or negative. For each model, we let 500 walkers move 20 000 steps, with an arbitrary 1000 step burn-in. We do not fit for periodic trends in this study due to the sparse data coverage.

The difference in strength between the two models was quantified by employing both the Bayesian Information Criterion (BIC; G. Schwarz 1978) and Akaike Information Criterion (AIC; H. Akaike 1974). These excel in testing the strength of the fits to the data, whilst also penalizing overly complex higher order polynomials. The AIC and BIC were computed with

$$\mathrm{AIC} = \chi^2 + 2(n+1) \tag{6}$$

and

$$\mathrm{BIC} = \chi^2 + \ln(N)(n+1) \tag{7}$$

for each model, where n is the polynomial degree, N is the number of data points, and χ^2 was calculated from each model using

$$\chi^2 = \sum_{i=1}^{N} \left(\frac{T_{\mathrm{obs},i} - T_{\mathrm{calc},i}}{\sigma_{\mathrm{obs},i}} \right)^2 \tag{8}$$

similarly to equation (2) in K. C. Patra et al. (2020). A list of all statistical quantities from the fits is displayed in Table 2, and linear residuals are plotted against the best fit in Fig. 2. We compared the two models by subtracting the quadratic BIC and AIC from their linear counterparts. Thus, a significant positive ΔBIC and ΔAIC should imply the presence of TTVs. The range of values of ΔBIC and ΔAIC that indicate a significant preference for one model over another is hard to define, so we required $\Delta\mathrm{BIC} \geq 10$ and $\Delta\mathrm{AIC} \geq 10$ to accept the quadratic model in preference to the linear one (e.g. R. E. Kass & A. E. Raftery 1995).

3.4 Tidal quality factor

We determined a lower bound on the modified tidal quality factor as an indication of the efficiency of tidal dissipation within the star, and its influence over the planet's orbit. Based on results from J. L. Birkby et al. (2014), G. Maciejewski et al. (2018), and others, and the formulation by P. Goldreich & S. Soter (1966), we use the following equation for the modified tidal quality factor:

$$Q'_\star = -\left(\frac{27\pi}{2}\right)\left(\frac{M_\mathrm{p}}{M_\star}\right)\left(\frac{R_\star}{a}\right)^5 \dot{P}^{-1} \tag{9}$$

where $\dot{P}$ is the rate of change of the orbital period. All other parameters have their former meanings. The lower limit on $Q'_\star$ for each stellar host was obtained by implementing the 3σ lower uncertainty of $\dot{P}$ into the above equation, given the relationship $Q'_\star \propto \dot{P}^{-1}$. Limits on $Q'_\star$ for the four objects are shown in Table 2. Note that this tidal quality factor represents only the stellar tidal dissipation and is independent of any dissipation within the planet.

3.5 Theoretical predictions

Our lower bound constraints on $Q'_\star$ for each of the four systems can be compared to theoretical predictions. The most efficient tidal mechanism in each case is predicted to be dissipation of internal gravity waves (part of the dynamical tide response) in their radiative cores, which are launched and propagate inwards from the radiative/convective boundary. If these waves are fully damped (by whatever mechanism) we can readily predict the resulting tidal dissipation and hence $Q'_\star$ (e.g. using equation 41 in A. J. Barker 2020). This regime is likely to be relevant if the planetary mass is large enough to cause the waves to break in the stellar core (e.g. A. J. Barker & G. I. Ogilvie 2010), though there are other possibilities, including gradual radiative damping of the waves leading to spin-up of the central portions of the star and the subsequent efficient wave absorption (e.g. Z. Guo, G. I. Ogilvie & A. J. Barker 2023), other strong wave–wave interactions (e.g. N. N. Weinberg et al. 2024), or sufficiently strong magnetic fields

Table 2. Parameters and statistical outputs of the linear and quadratic fits for each hot Jupiter.

HIP 65 Ab		
Quantity	Linear model	Quadratic model
T_0 (BJD)	2459540.547764(42)	2459540.547697(64)
P (d)	0.980972186(48)	0.980972242(63)
p (d)	–	$(1.16 \pm 0.84) \times 10^{-10}$
$\dot{P}$ (ms yr^{-1})	–	7.5 ± 5.4
$N_{\rm dof}$	27	26
χ^2	49.9	48.0
BIC	60.0	61.5
AIC	55.9	56.0
log $Q'_{*,\rm min}$	–	5.16 ± 0.04
NGTS-6 b		
Quantity	Linear model	Quadratic model
T_0 (BJD)	2459550.679388(94)	2459550.67962(14)
P (d)	0.88205815(11)	0.88205809(11)
p (d)	–	$(-2.9 \pm 1.2) \times 10^{-10}$
$\dot{P}$ (ms yr^{-1})	–	-20.6 ± 8.8
$N_{\rm dof}$	23	22
χ^2	66.0	60.5
BIC	75.7	73.4
AIC	72.0	68.5
log $Q'_{*,\rm min}$	–	4.28 ± 0.06
NGTS-10 b		
Quantity	Linear model	Quadratic model
T_0 (BJD)	2460035.788622(83)	2460035.78876(10)
P (d)	0.766893317(50)	0.76689297(17)
p (d)	–	$(-1.39 \pm 0.66) \times 10^{-10}$
$\dot{P}$ (ms yr^{-1})	–	-11.5 ± 5.4
$N_{\rm dof}$	10	9
χ^2	17.6	13.0
BIC	25.0	23.0
AIC	23.6	21.0
log $Q'_{*,\rm min}$	–	4.93 ± 0.19
WASP-173 Ab		
Quantity	Linear model	Quadratic model
T_0 (BJD)	2459486.704505(71)	2459486.704763(98)
P (d)	1.38665315(11)	1.38665272(15)
p (d)	–	$(-7.3 \pm 1.9) \times 10^{-10}$
$\dot{P}$ (ms yr^{-1})	–	-33.2 ± 8.7
$N_{\rm dof}$	17	16
χ^2	58.0	43.5
BIC	66.8	55.3
AIC	64.0	51.5
log $Q'_{*,\rm min}$	–	4.47 ± 0.12

(though this is expected to be more relevant for F-stars; e.g. C. D. Duguid et al. 2024).

We have computed MESA stellar models and the resulting tidal gravity wave $Q'_\star$ for each of these systems (NGTS-6b and 10b were previously presented in A. J. Barker 2020). For HIP 65 A, we used a mass 0.781 $M_\odot$ and rotation period of 13.2 d (L. D. Nielsen et al. 2020), and for WASP-173 A, we used a mass 1.05 $M_\odot$ (C. Hellier et al. 2019) and rotation period of 8.4 d (E. Knudstrup et al. 2024) (both with initial metallicity $Z = 0.02$). We find $Q'_\star \approx 1.2 \times 10^5$ (at age 4.1 Gyr; L. D. Nielsen et al. 2020) to be applicable for HIP 65 Ab's orbital decay, and $Q'_\star \approx 2 - 6.3 \times 10^5$ (at ages 3–7 Gyr, with smaller values for older stars) for WASP-173 Ab. Both NGTS-6b and NGTS-10b are predicted to have $Q'_\star \approx 1 \times 10^5$ relevant for their orbital decay at ages of approximately 10 Gyr (A. J. Barker 2020). These predictions assume the gravity waves to be fully damped, and much larger values ($> 10^9$) would be expected if the waves are only weakly damped by radiative diffusion (unless the system happens to excite a g mode in resonance, which has a low probability). Wave breaking is predicted for the expected ages of WASP-173 A (i.e. at 3–7 Gyr, with C. Hellier et al. 2019 finding 7 ± 3 Gyr and J. Labadie-Bartz et al. 2019 finding $1.5 - 5.0$ Gyr), so this regime is plausibly justified in this system, though it is less clear in the others, none of which clearly satisfy the criterion for wave breaking (in section 3.2 of A. J. Barker 2020).

4 RESULTS AND DISCUSSION

A transit-timing analysis was carried out on four hot-Jupiter systems: HIP 65 A, NGTS-6, NGTS-10, and WASP-173 A. Their large mass ratios, short periods, and large fractional radii made these planets excellent candidates for the detection of tidal decay. We collected a total of 33 transit times of our own from ground-based observations using the 1.54-m Danish Telescope, 24 from *TESS* (two per sector), 21 from the literature, and 7 from the ETD. The time baselines covered by all data used in this study are 6.4, 7, 8.7, and 9 yr for HIP 65 Ab, NGTS-6b, NGTS-10b, and WASP-173 Ab, respectively. The results from our analyses are tabulated in Table 2 and displayed visually in Fig. 2. Tables containing all timing data used in this study are located in Appendix B.

4.1 HIP 65 Ab

From the orbital decay model, we find a positive quadratic coefficient, corresponding to a period increase of 7.5 ± 5.4 ms yr^{-1}. For comparison, the published period derivatives for HIP 65 Ab are 22.3 ± 9.6 ms yr^{-1} from E. R. Adams et al. (2024) and a rate of period change per cycle of $(-0.1 \pm 3.1) \times 10^{-10}$ d by G. Maciejewski et al. (2024). Our result is consistent with these but also with a constant period at under 2σ. The statistical analysis shows no substantial favouring of either model, with ΔBIC $= -1.5$ and ΔAIC $= -0.1$, acting as sufficient reason not to explore models with higher order polynomials. The detection of any orbital decay in this system would require observations over a longer time span than currently available.

4.2 NGTS-6 b

We find the difference between the strength of the linear and quadratic models to be ΔBIC $= 2.3$ and ΔAIC $= 3.5$, which does not significantly favour the quadratic model. Alongside an inspiral rate of -21 ± 9 ms yr^{-1}, tidal decay is not significantly favoured over the constant-period alternative. Although the best-fitting value is negative, this result is consistent with zero at 2.3σ and therefore does not directly imply a shrinking orbit. Further observations will be paramount in distinguishing orbital decay from typical orbital motion. Opportunely, NGTS-6 b is in a sample of ~ 100 known transiting exoplanets that will be observed by the *PLATO* mission (H. Rauer et al. 2025) in its first long-pointing field (LOPS2; V. Nascimbeni et al. 2025). As a result, the occasion may present itself in less than a decade with the release of *PLATO* data. This planet makes an interesting tidal decay candidate for future study.

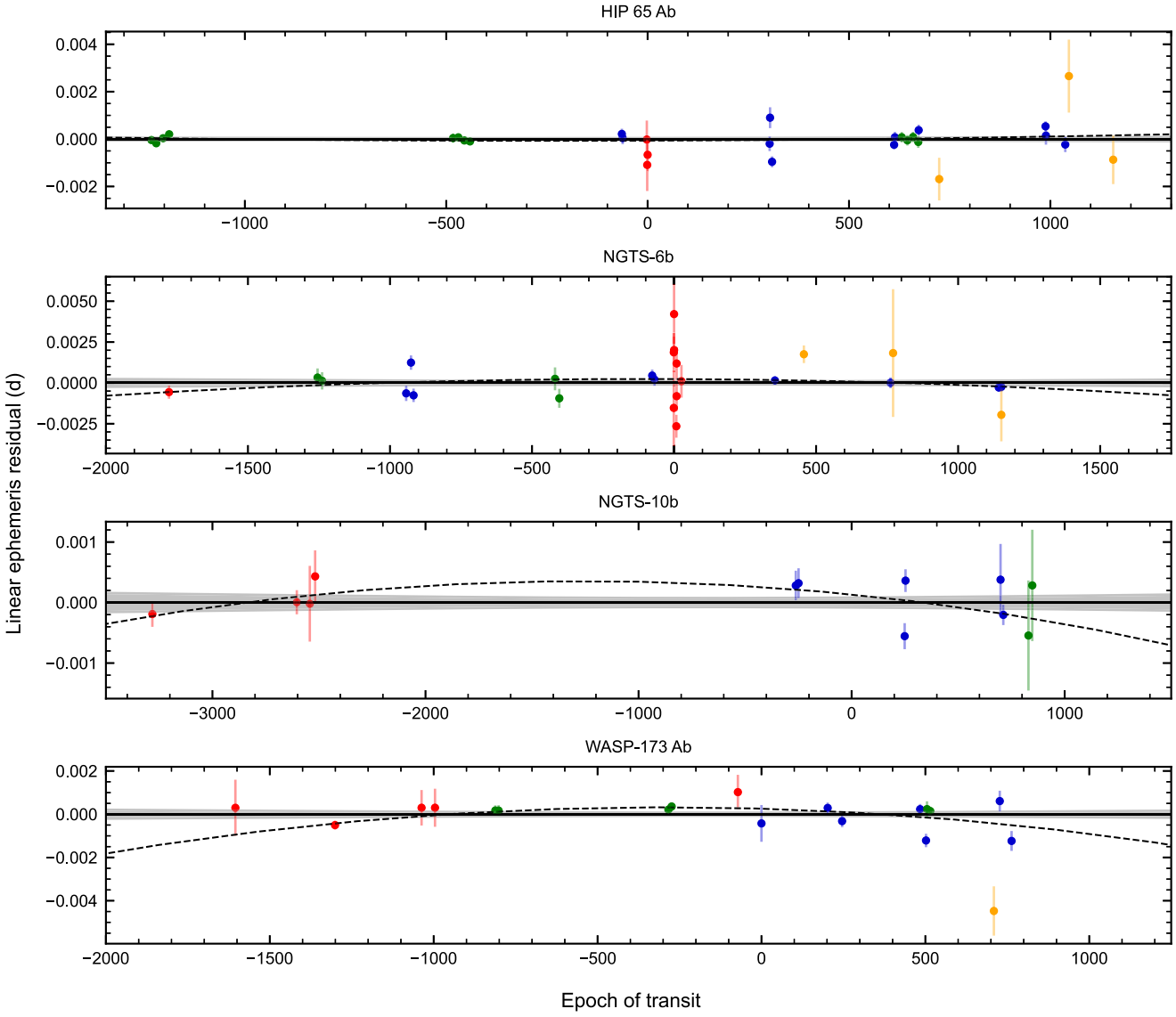

Figure 2. Linear ephemeris residuals plotted against the number of cycles from the median time. The solid line at $y = 0$ represents the linear model, where the shaded grey region is its 1σ error. The dashed line represents the quadratic model in terms of the linear residuals. Blue points denote new transit times from the Danish Telescope. Green points denote *TESS* transits. Red points denote transit times from the literature. Orange points denote times from the ETD.

4.3 NGTS-10 b

A successful transit-timing analysis of NGTS-10 is hindered by the lack of available transit times. Although the times used in this study span over eight years, only 12 transit times have been obtained. The $\dot{P}$ value presented here is negative with a significance of just above 2σ based on the available data. There is a gap of several years between the earlier times and the observations presented in the current work (see Fig. 2), meaning that a linear ephemeris is precisely anchored but that the quadratic term is not well constrained.

Without precise points in the epoch space between the original discovery observations and the first Danish Telescope observation, this decay rate could vary significantly in either direction. The status of orbital decay in this system will be helped by new timing data, particularly as this planet is also in the *PLATO* LOPS2 field (V. Nascimbeni et al. 2025) and has planned observations with the *James Webb Space Telescope* (J. P. Gardner et al. 2006; Q. Changeat et al. 2024). Although theoretical studies provide conflicting evidence for the rate of tidal dissipation (e.g. A. J. Barker 2020; T. Tokuno et al. 2024), longer photometric coverage will be beneficial in constraining $\dot{P}$ even should it be consistent with zero. As of now, NGTS-10 b still remains a good candidate.

4.4 WASP-173 Ab

Our timing analysis of WASP-173 Ab produced a lower $\dot{P}$ and p than those detected in other works, with E. R. Adams et al. (2024) finding $\dot{P} = 19.3 \pm 11.0\,\mathrm{ms\,yr^{-1}}$ and G. Maciejewski et al. (2024) finding $p = (0.6 \pm 2.6) \times 10^{-10}$. The differences are likely attributed to the variety of data sources used in each work. We find $\Delta\mathrm{BIC} = 11.5$ and $\Delta\mathrm{AIC} = 12.5$, indicating the quadratic model fits the residuals better than that of the linear. Although $\dot{P}$ is negative at 3.8σ, this result could be optimistic, caused by underestimated uncertainties on some of the transit times. The orbital decay scenario is still not conclusive. Nevertheless, G. Maciejewski et al. (2024) predict wave breaking provided the stellar host is older than ~ 4.5 Gyr, giving the theoretical

constraint $Q'_\star < 1.5 \times 10^6$ which agrees with our own theoretical estimation. As with the other three systems, more timing data spanning a longer time interval will be needed to identify orbital decay in WASP-173 A.

5 CONCLUSIONS

By taking the 3σ lower limits of $\dot{P}$ for each system, we computed lower limits for $Q'_\star$. These are not remarkable, approximately lying in the range $10^4 < Q'_{\star,\min} < 10^5$, but are compatible with our theoretical predictions if tidally-driven orbital decay due to gravity waves is actually occurring. Given that the current constraints are not very far from predictions, each of these four systems would be promising for future follow-up studies since they have very good potential to test tidal theory. On the other hand, the possible outward migration of HIP 65 Ab, if confirmed in future studies, would be more difficult to explain by tidal processes alone in such a slowly rotating star. A significant positive $\dot{P}$, if found, would be most likely explained by another phenomenon, such as the light time effect (e.g. E. Yang, Y. Su & J. N. Winn 2025) or an acceleration of the system away from the observer. As of now, our TTV models show no conclusive evidence for orbital decay in any of these systems. WASP-173 Ab has the strongest suggestion of orbital decay and is a promising candidate for future studies.

The data we presented and analysed in the current work will be valuable for future studies of these objects. Long-term monitoring of all four planetary systems will be useful in progressively constraining $Q'_\star$ and ultimately leading to a significant detection of tidal effects.

ACKNOWLEDGEMENTS

JS acknowledges support from STFC under grant no. ST/Y002563/1. FA, MA, and UGJ acknowledge funding from the Novo Nordisk Foundation Interdisciplinary Synergy Programme grant no. NNF19OC0057374. VB and PR are supported by PRIN 2022 CUP D53D23002590006. RFJ acknowledges the support provided by the GEMINI/ANID project under grant no. 32240028, by ANID's Millennium Science Initiative through grant ICN12_009, awarded to the Millennium Institute of Astrophysics (MAS), and by ANID's Basal project FB210003. EK is supported by the National Research Foundation of Korea 2021M3F7A1082056. LM acknowledges the financial contribution from PRIN MUR 2022 project 2022J4H55R. This paper includes data collected by the *TESS* mission and obtained from the MAST data archive at the Space Telescope Science Institute (STScI). Funding for the *TESS* mission is provided by the NASA's Science Mission Directorate. STScI is operated by the Association of Universities for Research in Astronomy, Inc., under NASA contract NAS 5–26555. This work has made use of data from the European Space Agency (ESA) mission *Gaia*,[4] processed by the *Gaia* Data Processing and Analysis Consortium DPAC[5]). Funding for the DPAC has been provided by national institutions, in particular the institutions participating in the *Gaia* Multilateral Agreement. This research has received funding from the Europlanet 2024 Research Infrastructure (RI) programme. The Europlanet 2024 RI provides free access to the world's largest collection of planetary simulation and analysis facilities, data services and tools, a ground-based observational network and programme of community support activities. Europlanet 2024 RI has received funding from the European Union's Horizon 2020 research and innovation programme under grant agreement no. 871149.

The following resources were used in the course of this work: the NASA Astrophysics Data System; the SIMBAD database operated at CDS, Strasbourg, France; and the arχiv scientific paper preprint service operated by Cornell University.

This work is based on data collected by MiNDSTEp with the Danish 1.54-m Telescope at the ESO La Silla Observatory in Chile. The operation, servicing, and maintenance of the DK-1.54-m Telescope is supported by a Villum Young Investigator grant (project no. 25501) and a Villum Experiment grant (VIL69896) from VILLUM FONDEN.

[4] https://www.cosmos.esa.int/gaia

[5] https://www.cosmos.esa.int/web/gaia/dpac/consortium

DATA AVAILABILITY

The light curves obtained with the Danish Telescopes will be made available at the Centre de Données astronomiques de Strasbourg (CDS) at http://cdsweb.u-strasbg.fr/. The *TESS* data used in this article are available in the MAST archive (https://mast.stsci.edu/portal/Mashup/Clients/Mast/Portal.htm).

REFERENCES

Adams E. R. et al., 2024, Planet. Sci. J., 5, 163
Agol E., Fabrycky D. C., 2018, in Deeg H. J., Belmonte J. A. eds, Handbook of Exoplanets, Springer International Publishing AG, Cham, p. 7
Akaike H., 1974, IEEE Trans. Autom. Control, 19, 716
Akinsanmi B. et al., 2024, A&A, 685, A63
Alvarado-Montes J. A., Sucerquia M., García-Carmona C., Zuluaga J. I., Spitler L., Schwab C., 2021, MNRAS, 506, 2247
Antonetti V., Goodman J., 2022, ApJ, 939, 91
Applegate J. H., 1992, ApJ, 385, 621
Bai L., Gu S., Wang X., Sun L., Kwok C.-T., Hui H.-K., 2022, MNRAS, 512, 3113
Barker A. J., 2020, MNRAS, 498, 2270
Barker A. J., Ogilvie G. I., 2010, MNRAS, 404, 1849
Baştürk Ö. et al., 2025, MNRAS, 541, 714
Bernabò L. M. et al., 2025, A&A, 694, A233
Birkby J. L. et al., 2014, MNRAS, 440, 1470
Bouma L. G. et al., 2019, AJ, 157, 217
Bouma L. G., Winn J. N., Howard A. W., Howell S. B., Isaacson H., Knutson H., Matson R. A., 2020, ApJ, 893, L29
Changeat Q., Ito Y., Al-Refaie A. F., Yip K. H., Lueftinger T., 2024, AJ, 167, 195
Claret A., Southworth J., 2022, A&A, 664, A128
Counselman C. C., 1973, ApJ, 180, 307
Demory B.-O., Seager S., 2011, ApJS, 197, 12
Dominik M. et al., 2010, Astron. Nachr., 331, 671
Duguid C. D., de Vries N. B., Lecoanet D., Barker A. J., 2024, ApJ, 966, L14
Eastman J., Siverd R., Gaudi B. S., 2010, PASP, 122, 935
Foreman-Mackey D. et al., 2013, Astrophysics Source Code Library, record ascl:1303.002
Gal-on E., Hamrick A., Kim E., Owens X., 2022, in Martin J. C., Buchheim R. K., Gill R. M., Green W., Menke J. eds, 41st Annual Conference of the Society for Astronomical Sciences (SAS-2022). The Symposium on Telescope Science, Ontario, Canada, p. 7
Gardner J. P. et al., 2006, Space Sci. Rev., 123, 485
Gaudi B. S. et al., 2002, ApJ, 566, 463
Goldreich P., Soter S., 1966, Icarus, 5, 375
Guo Z., Ogilvie G. I., Barker A. J., 2023, MNRAS, 521, 1353
Harre J.-V., Smith A. M. S., 2023, Universe, 9, 506
Hebb L. et al., 2009, ApJ, 693, 1920
Hellier C. et al., 2019, MNRAS, 482, 1379

Helling C. et al., 2023, A&A, 671, A122
Hestroffer D., 1997, A&A, 327, 199
Howard A. W. et al., 2010, Science, 330, 653
Howard A. W. et al., 2012, ApJS, 201, 15
Hut P., 1980, A&A, 92, 167
Hut P., 1981, A&A, 99, 126
Irwin J. B., 1952, ApJ, 116, 211
Ivshina E. S., Winn J. N., 2022, ApJS, 259, 62
Kappelmeier J. A., MacDonald R. J., Lewis N. K., 2024, ApJ, 975, 61
Kass R. E., Raftery A. E., 1995, J. Am. Stat. Assoc., 90, 773
Knudstrup E. et al., 2024, A&A, 690, A379
Kokori A. et al., 2022a, Exp. Astron., 53, 547
Kokori A. et al., 2022b, ApJS, 258, 40
Kokori A. et al., 2023, ApJS, 265, 4
Kutluay A. C., Basturk O., Yalçinkaya S., Saguner Rambaldi T., Yerli S. K., 2023, Turkish J. Astron. Astrophys., 4, 10
Labadie-Bartz J. et al., 2019, ApJS, 240, 13
Leonardi P. et al., 2024, A&A, 686, A84
Levrard B., Winisdoerffer C., Chabrier G., 2009, ApJ, 692, L9
Lightkurve Collaboration, 2018, Astrophysics Source Code Library, record ascl:1812.013
Liu Q., Zhu W., Masuda K., Libby-Roberts J. E., Bello-Arufe A., Cañas C. I., 2024, ApJ, 976, L14
Love A. E. H., 1911, Some Problems of Geodynamics. Cambridge University Press, Cambridge
Maciejewski G. et al., 2016, A&A, 588, L6
Maciejewski G. et al., 2018, Acta Astron., 68, 371
Maciejewski G., Golonka J., Fernández M., Ohlert J., Casanova V., Pérez Medialdea D., 2024, A&A, 692, A35
Mancini L. et al., 2022, MNRAS, 509, 1447
Maxted P. F. L., Serenelli A. M., Southworth J., 2015, A&A, 577, A90
Mayor M. et al., 2011 , preprint (arXiv:1109.2497)
McCormac J. et al., 2020, MNRAS, 493, 126
Murray C. D., Dermott S. F., 1999, Tides, Rotation, and Shape. Cambridge University Press, Cambridge, p. 130
Nascimbeni V. et al., 2025, A&A, 694, A313
Nediyedath A. S. et al., 2023, J. Am. Assoc. Var. Star Observ., 51, 243
Nielsen L. D. et al., 2020, A&A, 639, A76
Ogilvie G. I., 2014, ARA&A, 52, 171
Paredes L. A., Henry T. J., Quinn S. N., Gies D. R., Hinojosa-Goñi R., James H.-S., Jao W.-C., White R. J., 2021, AJ, 162, 176
Patra K. C. et al., 2020, AJ, 159, 150
Poddaný S., Brát L., Pejcha O., 2010, New Astron., 15, 297
Price E. M., Becker J., de Beurs Z. L., Rogers L. A., Vanderburg A., 2025, ApJ, 981, L7
Rasio F. A., Tout C. A., Lubow S. H., Livio M., 1996, ApJ, 470, 1187
Rauer H. et al., 2025, Exp. Astron., 59, 26
Ricker G. R. et al., 2015, J. Astron. Telesc. Instrum. Syst., 1, 014003
Savitzky A., Golay M. J. E., 1964, Anal. Chem., 36, 1627
Schwarz G., 1978, Ann. Stat., 6, 461
Shan S.-S. et al., 2023, ApJS, 264, 37
Southworth J. et al., 2009a, MNRAS, 396, 1023
Southworth J. et al., 2009b, MNRAS, 399, 287
Southworth J. et al., 2014, MNRAS, 444, 776
Southworth J. et al., 2019, MNRAS, 490, 4230
Southworth J. et al., 2022, MNRAS, 515, 3212
Southworth J., 2008, MNRAS, 386, 1644
Southworth J., 2013, A&A, 557, A119
Stetson P. B., 1987, PASP, 99, 191
Szabó G. M., Kiss L. L., 2011, ApJ, 727, L55
Tejada Arevalo R. A., Winn J. N., Anderson K. R., 2021, ApJ, 919, 138
Tokuno T., Fukui A., Suzuki T. K., 2024, ApJ, 973, 128
Turner J. D., Flagg L., Ridden-Harper A., Jayawardhana R., 2022, AJ, 163, 281
Turner J. D., Ridden-Harper A., Jayawardhana R., 2021, AJ, 161, 72
Vines J. I. et al., 2019, MNRAS, 489, 4125
Wang G., Espinoza N., 2024, AJ, 167, 1
Wang W., Zhang Z., Chen Z., Wang Y., Yu C., Ma B., 2024, ApJS, 270, 14
Weinberg N. N., Davachi N., Essick R., Yu H., Arras P., Belland B., 2024, ApJ, 960, 50
Wilson D. M. et al., 2008, ApJ, 675, L113
Winn J. N., Stefánsson G., 2025, preprint (arXiv:2510.05229)
Wong I., Shporer A., Vissapragada S., Greklek-McKeon M., Knutson H. A., Winn J. N., Benneke B., 2022, AJ, 163, 175
Wright J. T., Marcy G. W., Howard A. W., Johnson J. A., Morton T. D., Fischer D. A., 2012, ApJ, 753, 160
Yang E., Su Y., Winn J. N., 2025, ApJ, 986, 117
Yee S. W. et al., 2020, ApJ, 888, L5
Zanazzi J. J., Chiang E., 2025, ApJ, 983, 157

APPENDIX A: TRANSIT LIGHT CURVES FROM *TESS*

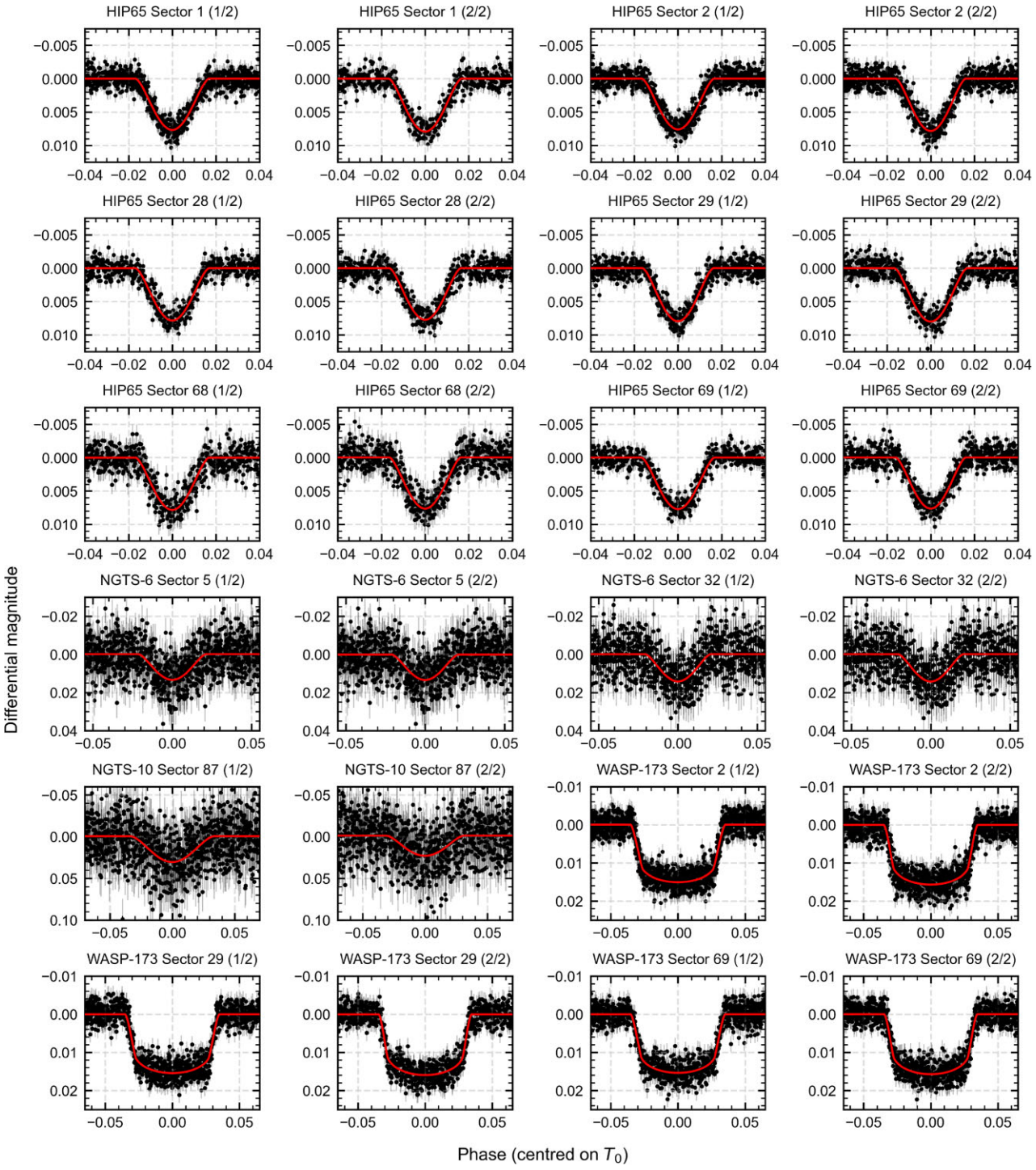

Figure A1. Phase-folded transit light curves for HIP 65 A, NGTS-6, NGTS-10, and WASP-173 A taken from *TESS*. Data points are displayed with their error bars. Fits are plotted in front of the data. The *TESS* sectors are displayed above each plot. 1/2 refers to the first half of a sector. 2/2 refers to the second half of a sector.

APPENDIX B: TIMING DATA USED IN THIS WORK

Table B1. Times of mid-transit for HIP 65 A used in this study.

BJD(TDB)	Epoch	Residuals (d)	Source
2458331.98999±0.00012	−1232.0	−0.00004	This work (*TESS*)
2458343.76152±0.00015	−1220.0	−0.00018	This work (*TESS*)
2458360.43826±0.00011	−1203.0	+ 0.00004	This work (*TESS*)
2458375.15301±0.00012	−1188.0	+ 0.00020	This work (*TESS*)
2459066.73824±0.00019	−483.0	+ 0.00004	This work (*TESS*)
2459079.49091±0.00015	−470.0	+ 0.00007	This work (*TESS*)
2459094.20536±0.00015	−455.0	−0.00006	This work (*TESS*)
2459107.93893±0.00013	−441.0	−0.00010	This work (*TESS*)
2459477.76576±0.00022	−64.0	+ 0.00022	This work (Danish Telescope)
2459479.72753±0.00026	−62.0	+ 0.00004	This work (Danish Telescope)
2459538.58580±0.00080	−2.0	−0.00002	A. Kokori et al. (2023)
2459539.56570±0.00110	−1.0	−0.00109	A. Kokori et al. (2023)
2459540.54710±0.00070	0.0	−0.00066	A. Kokori et al. (2023)
2459837.78214±0.00031	303.0	−0.00020	This work (Danish Telescope)
2459838.76421±0.00044	304.0	+ 0.00090	This work (Danish Telescope)
2459843.66721±0.00023	309.0	−0.00096	This work (Danish Telescope)
2460140.90250±0.00018	612.0	−0.00024	This work (Danish Telescope)
2460142.86476±0.00023	614.0	+ 0.00007	This work (Danish Telescope)
2460159.54129±0.00022	631.0	+ 0.00008	This work (*TESS*)
2460173.27477±0.00022	645.0	−0.00005	This work (*TESS*)
2460187.00852±0.00022	659.0	+ 0.00009	This work (*TESS*)
2460199.76095±0.00025	672.0	−0.00012	This work (*TESS*)
2460200.74242±0.00023	673.0	+ 0.00038	This work (Danish Telescope)
2460250.76994±0.00090	724.0	−0.00169	ETD
2460509.74882±0.00021	988.0	+ 0.00054	This work (Danish Telescope)
2460510.72940±0.00038	989.0	+ 0.00014	This work (Danish Telescope)
2460557.81569±0.00032	1037.0	−0.00023	This work (Danish Telescope)
2460566.64733±0.00154	1046.0	+ 0.00266	ETD
2460674.55074±0.00103	1156.0	−0.00087	ETD

Table B2. Times of mid-transit for NGTS-6 used in this study.

BJD(TDB)	Epoch	Residuals (d)	Source
2457982.37942±0.00040	−1778.0	−0.00056	This work (J. I. Vines et al. 2019)
2458443.69673±0.00056	−1255.0	+ 0.00033	This work (*TESS*)
2458457.80946±0.00053	−1239.0	+ 0.00013	This work (*TESS*)
2458718.89791±0.00047	−943.0	−0.00064	This work (Danish Telescope)
2458733.89478±0.00044	−926.0	+ 0.00124	This work (Danish Telescope)
2458741.83130±0.00041	−917.0	−0.00076	This work (Danish Telescope)
2459181.09727±0.00070	−419.0	+ 0.00025	This work (*TESS*)
2459194.32695±0.00058	−404.0	−0.00094	This work (*TESS*)
2459482.76136±0.00037	−77.0	+ 0.00045	This work (Danish Telescope)
2459489.81758±0.00038	−69.0	+ 0.00020	This work (Danish Telescope)
2459549.79580±0.00230	−1.0	−0.00153	A. Kokori et al. (2023)
2459549.79920±0.00120	−1.0	+ 0.00187	A. Kokori et al. (2023)
2459550.68140±0.00080	0.0	+ 0.00201	A. Kokori et al. (2023)
2459550.68360±0.00180	0.0	+ 0.00421	A. Kokori et al. (2023)
2459557.73320±0.00070	8.0	−0.00265	A. Kokori et al. (2023)
2459558.61710±0.00090	9.0	−0.00081	A. Kokori et al. (2023)
2459558.61910±0.00100	9.0	+ 0.00119	A. Kokori et al. (2023)
2459573.61300±0.00100	26.0	+ 0.00010	A. Kokori et al. (2023)
2459863.81018±0.00025	355.0	+ 0.00015	This work (Danish Telescope)
2459953.78172±0.00054	457.0	+ 0.00175	ETD
2460222.80771±0.00033	762.0	+ 0.00001	This work (Danish Telescope)
2460230.74805±0.00391	771.0	+ 0.00183	ETD
2460558.87158±0.00024	1143.0	−0.00028	This work (Danish Telescope)
2460566.80843±0.00162	1152.0	−0.00196	ETD
2460566.81014±0.00030	1152.0	−0.00024	This work (Danish Telescope)

Table B3. Times of mid-transit for NGTS-10 used in this study.

BJD(TDB)	Epoch	Residuals	Source
2457518.84457±0.00021	−3282.0	−0.00019	This work (J. McCormac et al. 2020)
2458038.79843±0.00020	−2604.0	+ 0.00001	This work (J. McCormac et al. 2020)
2458085.57890±0.00063	−2543.0	−0.00002	This work (J. McCormac et al. 2020)
2458104.75168±0.00043	−2518.0	+ 0.00043	This work (J. McCormac et al. 2020)
2459834.86286±0.00024	−262.0	+ 0.00028	This work (Danish Telescope)
2459844.83251±0.00025	−249.0	+ 0.00032	This work (Danish Telescope)
2460226.74450±0.00022	249.0	−0.00056	This work (Danish Telescope)
2460229.81299±0.00019	253.0	+ 0.00036	This work (Danish Telescope)
2460571.84743±0.00059	699.0	+ 0.00038	This work (Danish Telescope)
2460581.81646±0.00017	712.0	−0.00020	This work (Danish Telescope)
2460672.30953±0.00091	830.0	−0.00054	This work (*TESS*)
2460686.11444±0.00092	848.0	+ 0.00028	This work (*TESS*)

Table B4. Times of mid-transit for WASP-173 A used in this study.

BJD(TDB)	Epoch	Residuals	Source
2457261.12650±0.00130	−1605.0	+ 0.00030	J. Labadie-Bartz et al. 2019
2457682.66826±0.00020	−1301.0	−0.00050	This work (C. Hellier et al. 2019)
2458048.74549±0.00082	−1037.0	+ 0.00030	J. Labadie-Bartz et al. 2019
2458105.59827±0.00088	−996.0	+ 0.00030	J. Labadie-Bartz et al. 2019
2458360.74232±0.00024	−812.0	+ 0.00017	This work (*TESS*)
2458374.60885±0.00025	−802.0	+ 0.00017	This work (*TESS*)
2459092.89522±0.00022	−284.0	+ 0.00021	This work (*TESS*)
2459106.76190±0.00019	−274.0	+ 0.00036	This work (*TESS*)
2459386.86650±0.00080	−72.0	+ 0.00102	A. Kokori et al. (2023)
2459486.70408±0.00085	0.0	−0.00043	This work (Danish Telescope)
2459766.80873±0.00025	202.0	+ 0.00029	This work (Danish Telescope)
2459827.82086±0.00028	246.0	−0.00032	This work (Danish Telescope)
2460157.84486±0.00024	484.0	+ 0.00023	This work (Danish Telescope)
2460182.80317±0.00031	502.0	−0.00121	This work (Danish Telescope)
2460186.96458±0.00036	505.0	+ 0.00024	This work (*TESS*)
2460200.83102±0.00020	515.0	+ 0.00014	This work (*TESS*)
2460469.83711±0.00114	709.0	−0.00447	ETD
2460494.80195±0.00048	727.0	+ 0.00061	This work (Danish Telescope)
2460544.71962±0.00046	763.0	−0.00124	This work (Danish Telescope)

[1]*Astrophysics Group, Keele University, Staffordshire ST5 5BG, UK*
[2]*Institute for Astronomy, University of Edinburgh, Royal Observatory, Edinburgh EH9 3HJ, UK*
[3]*Centre for Astrophysics Research, Department of Physics, Astronomy and Mathematics, University of Hertfordshire, College Lane, Hatfield AL10 9AB, UK*
[4]*Centre for ExoLife Sciences, Niels Bohr Institute, Jagtvej 155, DK-2200 Copenhagen, Denmark*
[5]*Cosmic Dawn Centre (DAWN), Niels Bohr Institute, Jagtvej 155, DK-2200 Copenhagen, Denmark*
[6]*Department of Applied Mathematics, School of Mathematics, University of Leeds, Leeds LS2 9JT, UK*
[7]*INAF – Osservatorio Astrofisico di Torino, Via Osservatorio 20, I-10025, Pino Torinese, Italy*
[8]*Dipartimento di Fisica 'E.R. Caianiello', Università di Salerno, Via Giovanni Paolo II 132, I-84084 Fisciano, Italy*
[9]*Istituto Nazionale di Fisica Nucleare, Sezione di Napoli, Via Cintia, I-80126 Napoli, Italy*
[10]*Universität Hamburg, Faculty of Mathematics, Informatics and Natural Sciences, Department of Earth Sciences, Meteorological Institute, Bundesstraße 55, D-20146 Hamburg, Germany*
[11]*Alma Mater Studiorum – University of Bologna, Dipartimento di Fisica e Astronomia 'Augusto Righi', Via Gobetti 93/2, I-40129 Bologna, Italy*
[12]*Centre for Exoplanet Science, SUPA, School of Physics & Astronomy, University of St Andrews, North Haugh, St Andrews KY16 9SS, UK*
[13]*Instituto de Astronomia y Ciencias Planetarias, Universidad de Atacama, Copayapu 485, 1531772, Copiapo, Chile*
[14]*Millennium Institute of Astrophysics MAS, Nuncio Monsenor Sotero Sanz 100, Of. 104, Providencia, 7510109, Santiago, Chile*
[15]*Instituto de Astrofísica, Facultad de Física, Pontificia Universidad Católica de Chile, Av. Vicuña Mackenna 4860, 7820436 Macul, Santiago, Chile*
[16]*Department of Physics, University of Southern Denmark, Chemistry and Pharmacy, SDU-Galaxy, Campusvej 55, DK-5230, Odense M, Denmark*
[17]*Astronomisches Rechen-Institut, Zentrum für Astronomie der Universität Heidelberg (ZAH), D-69120 Heidelberg, Germany*
[18]*Astronomy Research Center, Research Institute of Basic Sciences, Seoul National University, 1 Gwanak-ro, Gwanak-gu, Seoul 08826, Korea*
[19]*Centro de Astronomía, Universidad de Antofagasta, Av. Angamos 601, 02800, Antofagasta, Chile*

[20]*Dipartimento di Fisica, Università degli Studi di Roma Tor Vergata, via della Ricerca Scientifica 1, I-00133 Roma, Italy*
[21]*Max Planck Institute for Astronomy, Königstuhl 17, D-69117, Heidelberg, Germany*
[22]*Instituto de Astrofísica e Ciências do Espaço, Departamento de Física, Universidade de Coimbra, 3040-004 Coimbra, Portugal*
[23]*Departamento de Matemática y Física Aplicadas, Facultad de Ingeniería, Universidad Católica de la Santísima Concepción, Alonso de Rivera 2850, Concepción, Chile*
[24]*Perimeter Institute for Theoretical Physics, 31 Caroline St N, Waterloo, ON N2L 2Y5, Canada*
[25]*Centre for Electronic Imaging, Department of Physical Sciences, The Open University, Milton Keynes MK7 6AA, UK*

This paper has been typeset from a TEX/LATEX file prepared by the author.